Calculation of Divergent Channel Flows with a Multiple-Time-Scale Turbulence Model

S.-W. Kim*
NASA Lewis Research Center, Cleveland, Ohio 44135

Numerical calculations of turbulent reattaching shear layers in a divergent channel are presented. The turbulence is described by a multiple-time-scale turbulence model. The turbulent flow equations are solved by a control-volume-based finite-difference method. The computational results are compared with those obtained using k-ϵ turbulence models and algebraic Reynolds stress turbulence models. It is shown that the multiple-time-scale turbulence model yields significantly improved computational results compared with the other turbulence models in the region where the turbulence is in a strongly nonequilibrium state.

Nomenclature

A_u = coefficient for tangential velocity correction
A_v = coefficient for transverse velocity correction
c_f = friction coefficient, $= \tau_w/(0.5\rho U_\infty^2)$
c_p = pressure coefficient, $= p/(0.5\rho U_\infty^2)$
c_{pl}, c_{tl} = turbulence model constants for ϵ_p and ϵ_t equations, respectively, $l = 1, 3$
$c_{\mu f}$ = constant coefficient, $= 0.09$
f_μ = wall-damping function for eddy viscosity equation
f_ϵ = wall-damping function for near-wall dissipation rate
H = height of backward-facing step
k = turbulent kinetic energy, $= k_p + k_t$
k_p, k_t = turbulent kinetic energy of eddies in production and dissipation ranges, respectively
p = pressure
p' = incremental pressure
P_r = production rate of turbulent kinetic energy
R_t = turbulent Reynolds number, $= k^2/(\nu\epsilon_1)$
U_∞ = inlet flow velocity
u_j = time-averaged velocity, $= (u,v)$
u_τ = friction velocity, $= \sqrt{(\tau_w/\rho)}$
$\overline{u_i' u_j'}$ = Reynolds stress, $i = 1,2,3$ and $j = 1,2,3$
V = velocity vector, $= (u,v)$
x_j = spatial coordinates, $= x,y,z$
x_R = reattachment location
y^+ = wall coordinate, $= u_\tau y/\nu$
α = top-wall deflection angle, deg
ϵ_p = energy transfer rate from production range to dissipation range
ϵ_t = dissipation rate of turbulent kinetic energy
ϵ_1 = dissipation rate in near-wall region
κ = von Kármán constant, $= 0.41$
μ = molecular viscosity
μ_e = effective viscosity, $= \mu + \mu_t$
μ_t = turbulent viscosity
ν = kinematic viscosity of fluid
ν_t = turbulent eddy viscosity
ρ = density
$\sigma_{kp}, \sigma_{kt}, \sigma_{\epsilon p}, \sigma_{\epsilon t}$ = turbulent Prandtl number for k_p, k_t, ϵ_p and ϵ_t, respectively
τ_w = wall-shearing streess

Superscript
* = current value

Introduction

THE experimental study of reattaching shear layers in a divergent channel was designed to test the predictive capability of various turbulence models, to identify any deficiency in turbulence closure models, and thus to improve the predictive capability of turbulence models.[1] The flow geometry is shown in Fig. 1. The height of the backward-facing step is smaller than the boundary-layer thickness of the incoming flow. Abrupt breakdown of the boundary layer generated a strong nonequilibrium turbulent flow. Furthermore, a strong pressure gradient was generated by varying the divergence angle of the top wall to study its effect on the development of the turbulence field, especially the Reynolds stress, and the reattachment process. A number of turbulence models, such as k-ϵ turbulence models and algebraic Reynolds stress turbulence models (ARSM), were shown to yield poor computational results for the flow.[1] It is also shown in Ref. 1 that a modified ARSM yields computational results that are in good agreement with measured data. However, generality of the improved predictive capability for other complex turbulent flows has not been shown yet.

The single-time-scale turbulence models such as k-ϵ turbulence models, algebraic stress turbulence models, and Rey-

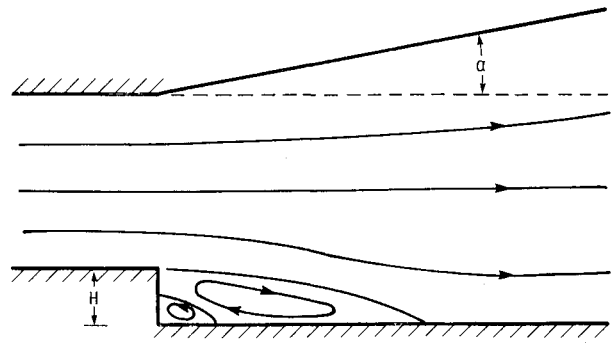

H: HEIGHT OF THE BACKWARD-FACING STEP, α: TOP WALL DEFLECTION ANGLE

Fig. 1 Nomenclature of the reattaching shear layer.

Received Oct. 16, 1989; revision received March 12, 1990.

*Research Associate, Institute for Computational Mechanics in Propulsion. Member AIAA.

nolds stress turbulence models yield reasonably accurate computational results for simple turbulent flows; however, the predictive capability degenerates rapidly as turbulent flows to be solved become more complex. The degenerated predictive capability is partly attributed to the use of a single time scale to describe both the turbulent transport of mass and momentum and the dissipation of the turbulent kinetic energy. In the multiple-time-scale turbulence models (hereafter abbreviated as the M-S turbulence models), the turbulent transport of mass and momentum is described using the time scale of the large eddies, and the dissipation rate is described using the time scale of the fine-scale eddies.[2-5] The M-S turbulence models proposed by Kim and Chen,[2] Hanjalic et al.,[3] and Schiestel[4] are based on the simplified split-spectrum method. In these turbulence models, the turbulence field is described by the four partial differential equations for the turbulent kinetic energy of large eddies (k_p), the turbulent kinetic energy of fine-scale eddies (k_t), the energy transfer rate (ϵ_p), and the dissipation rate (ϵ_t). On the other hand, in the multiscale turbulence model,[5-6] the turbulence field is described by the partial differential equations for the turbulent kinetic energy, the specific dissipation rate, and each component of the Reynolds stress tensor of the large eddies. Thus the multiscale turbulence model is quite different from the other M-S turbulence models even though the underlying physics may be similar.

It has been shown previously that the present M-S turbulence model[2] yields significantly improved computational results for a number of complex turbulent flows. On the other hand, the previous M-S turbulence model[3-4] did not quite come up to the expectations due to a few shortcomings in the closure model. These shortcomings and a few differences between the present M-S turbulence model and the other M-S turbulence model are discussed later in this paper. The complex turbulent flows to which the M-S turbulence model has been applied are summarized below.

Development of the mean velocity and turbulence fields in the wall-jet flow[7] and the wake boundary-layer interaction flow[8] depends mostly on the interaction of two turbulent shear layers. It is shown in Ref. 2 that the M-S turbulence model yields accurate computational results for these complex turbulent flows. It is also shown in Ref. 2 that the computational results for a backward-facing step flow[9] obtained using the M-S turbulence model compare somewhat more favorably with the measured data than those obtained using a Reynolds stress model. In the confined coaxial swirling jet,[10] the axial velocity in the center region is retarded by the influence of the swirl velocity, and a large reversed flow region is formed in the core region of the flow. Thus the flow is subjected to a large amount of streamline curvature. It can be found in Ref. 2 that the M-S turbulence model yields significantly improved computational results compared with those obtained using the standard k-ϵ turbulence model. Turbulent shear layers over curved surfaces are highly sensitive to the streamline curvature.[11,12] It can be found in Ref. 13 that the M-S turbulence model can predict the development of the internal layer and the separated flow regions in turbulent flows over a strongly curved surface, whereas the turbulence model incorporating a curvature correction method fails to predict the reversed flow regions. In numerical calculation of separated transonic turbulent flows over a curved hill,[14] a correct prediction of the separated flow field depends on the capability of a turbulence model to properly resolve the turbulence field subjected to extra strain rates caused by the streamline curvature and the shock-wave/boundary-layer interaction. It can be seen in Ref. 15 that the M-S turbulence model can predict the reversed flow region at low freestream Mach numbers, whereas various k-ϵ turbulence models fail to predict the reversed flow region. The M-S turbulence model also successfully predicted the extensive growth of the reversed flow region caused by the shock-wave/turbulent boundary-layer interaction at high freestream Mach numbers.[15]

In the present study, the near-wall turbulence is described by a "partially low Reynolds number" near-wall turbulence model.[16] In the model, only the turbulent kinetic energy equations are extended to include the near-wall low turbulence region, and the energy transfer rate and the dissipation rate inside the near-wall layer are obtained from algebraic equations. The algebraic equations were obtained from a k-equation turbulence model.[17] It would be appropriate to classify the model as a "partially low Reynolds number" near-wall model to distinguish it from other near-wall turbulence models such as wall functions, two-layer models, and low Reynolds number turbulence models. This class of near-wall turbulence model was first used in Chen and Patel[18] to solve turbulent flows over airfoils. Advantages of the partially low Reynolds number approach over the other methods can be summarized as follows. The turbulence length scale of the external flows is related to the flowfield characteristics.[19] On the other hand, the turbulence length scale of boundary-layer flows is strongly related to the normal distance from the wall. This characteristic of the wall-bounded turbulent flows can be described quite naturally by the partially low Reynolds number near-wall turbulence model. It is also interesting to note that various similar k-equation turbulence models, which form the basis of the present near-wall turbulence model, yield accurate computational results for various turbulent boundary-layer flows, turbulent flows with drag reduction, and fully developed unsteady turbulent pipe flows (see Ref. 16 for more details). However, the k-equation turbulence model itself is less useful for separated and/or swirling turbulent flows with complex geometry due to lack of a systematic method to evaluate the turbulence length scale. Development of the near-wall turbulence model and its application to fully developed turbulent channel and pipe flows can be found in Ref. 16. Incorporation of the near-wall turbulence model into a k-ϵ turbulence model and its application to a supersonic turbulent flow over a

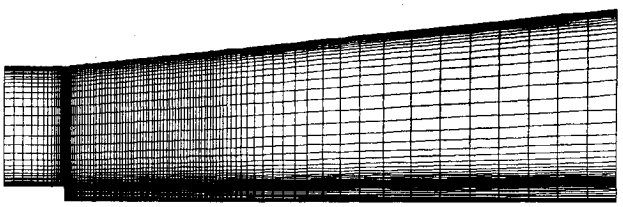

a) Entire domain

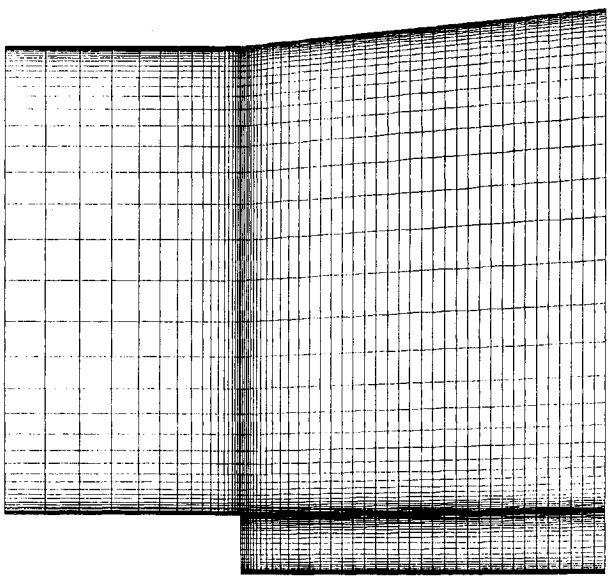

b) Vicinity of expansion corner

Fig. 2 Discretization of flow domain.

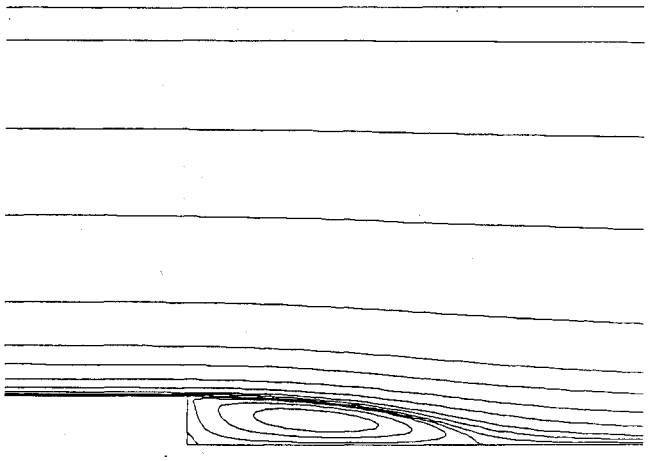

Fig. 3 Streamline contour.

compression ramp and a transonic flow over an axisymmetric curved hill can be found in Refs. 20 and 21, respectively.

The present numerical method is based on the pressure correction method[22] that has been used most extensively to solve incompressible flows whose domain can be discretized by an orthogonal mesh. However, the present numerical method is applicable for both incompressible and compressible flows with arbitrary, complex geometries. The capability to solve compressible flows is achieved by including convective incremental pressure terms into the pressure correction equation.[15,20] The accuracy and the convergence nature of the numerical method have been demonstrated by solving a number of flow cases. The example problems considered in Refs. 15 and 20 include a two-dimensional laminar flow in a channel with a 90-deg bend, polar cavity flows, a turbulent supersonic flow over a compression ramp, and a shock-wave/turbulent boundary-layer interaction in transonic flow over a curved hill.

Turbulent Flow Equations

The incompressible turbulent flow equations are given as

$$\frac{\partial}{\partial x}(\rho u)+\frac{\partial}{\partial y}(\rho v)=0 \tag{1}$$

$$\frac{\partial}{\partial x}(\rho uu)+\frac{\partial}{\partial y}(\rho vu)=\frac{\partial}{\partial x}\left(2\mu_e\frac{\partial u}{\partial x}\right)+\frac{\partial}{\partial y}\left[\mu_e\left(\frac{\partial u}{\partial y}+\frac{\partial v}{\partial x}\right)\right]-\frac{\partial}{\partial x}\left(p+\frac{2}{3}\rho k\right) \tag{2}$$

$$\frac{\partial}{\partial x}(\rho uv)+\frac{\partial}{\partial y}(\rho vv)=\frac{\partial}{\partial x}\left\{\mu_e\left(\frac{\partial u}{\partial y}+\frac{\partial v}{\partial x}\right)\right\}+\frac{\partial}{\partial y}\left(2\mu_e\frac{\partial v}{\partial y}\right)-\frac{\partial}{\partial y}\left(p+\frac{2}{3}\rho k\right) \tag{3}$$

where Eqs. (1-3) follow from the conservation of mass, u momentum, and v momentum, respectively. In numerical calculation, the conservation of mass equation is replaced by a pressure correction equation given as

$$\frac{\partial}{\partial x}\left(\rho A_u\frac{\partial p'}{\partial x}\right)+\frac{\partial}{\partial y}\left(\rho A_v\frac{\partial p'}{\partial y}\right)=\nabla\cdot(\rho V^*) \tag{4}$$

where the last term represents the mass imbalance. In the present numerical method, all flow variables, except pressure, are located at the same grid points and the pressure is located at the centroid of a cell formed by the four neighboring velocity grid points. A few remarks on the velocity-pressure decoupling[23] are in order for clarity. The discrete pressure correction equation obtained from Eq. (4), by treating it as a continuous form partial differential equation, becomes a five-diagonal system of equations for rectangular grids. This discrete pressure correction equation is strongly diagonally dominant even for highly skewed grids. Even the slightest symptom of velocity-pressure decoupling is not observed with the present pressure correction algorithm. On the other hand, the discrete pressure correction equation obtained by directly substituting the incremental-pressure/incremental-velocity relations into the conservation of mass equation as in the conventional pressure correction methods yields a nine-diagonal system of equations. This discrete pressure correction equation is not even diagonally dominant, and it can yield a velocity-pressure decoupled solution.[23] The strongly convergent nature of the present numerical method is partly attributed to the pressure correction algorithm that yields a strongly diagonally dominant system of equations even when a highly skewed mesh is used.[15,20] The discrete system of equations is solved using a tridiagonal matrix algorithm[22] with the off-diagonal terms moved to the load vector.

Turbulence Equations

For clarity, the M-S turbulence model supplemented with the near-wall turbulence model is summarized below. The turbulent kinetic energy and the energy transfer rate equations for the energy containing large eddies are given as

$$u_j\frac{\partial k_p}{\partial x_j}-\frac{\partial}{\partial x_j}\left[\left(\nu+\frac{\nu_t}{\sigma_{kp}}\right)\frac{\partial k_p}{\partial x_j}\right]=P_r-\epsilon_p \tag{5}$$

$$u_j\frac{\partial \epsilon_p}{\partial x_j}-\frac{\partial}{\partial x_j}\left[\left(\nu+\frac{\nu_t}{\sigma_{\epsilon p}}\right)\frac{\partial \epsilon_p}{\partial x_j}\right]=c_{p1}\frac{P_r^2}{k_p}+c_{p2}\frac{P_r\epsilon_p}{k_p}-c_{p3}\frac{\epsilon_p^2}{k_p} \tag{6}$$

where the production rate is given as

$$P_r=\nu_t\left[2\left(\frac{\partial u}{\partial x}\right)^2+2\left(\frac{\partial v}{\partial y}\right)^2+\left(\frac{\partial u}{\partial y}+\frac{\partial v}{\partial x}\right)^2\right]$$

The turbulent kinetic energy and the dissipation rate equations for the fine scale eddies are given as

$$u_j\frac{\partial k_t}{\partial x_j}-\frac{\partial}{\partial x_j}\left[\left(\nu+\frac{\nu_t}{\sigma_{kt}}\right)\frac{\partial k_t}{\partial x_j}\right]=\epsilon_p-\epsilon_t \tag{7}$$

$$u_j\frac{\partial \epsilon_t}{\partial x_j}-\frac{\partial}{\partial x_j}\left[\left(\nu+\frac{\nu_t}{\sigma_{\epsilon t}}\right)\frac{\partial \epsilon_t}{\partial x_j}\right]=c_{t1}\frac{\epsilon_p^2}{k_t}+c_{t2}\frac{\epsilon_p\epsilon_t}{k_t}-c_{t3}\frac{\epsilon_t^2}{k_t} \tag{8}$$

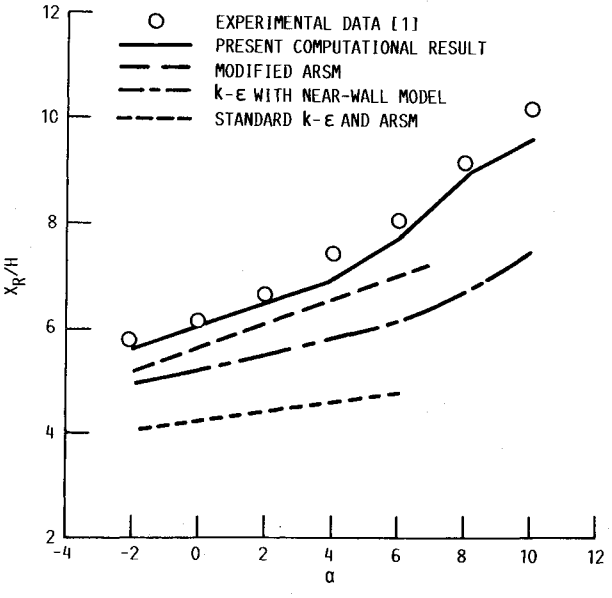

Fig. 4 Reattachment location vs deflection angle.

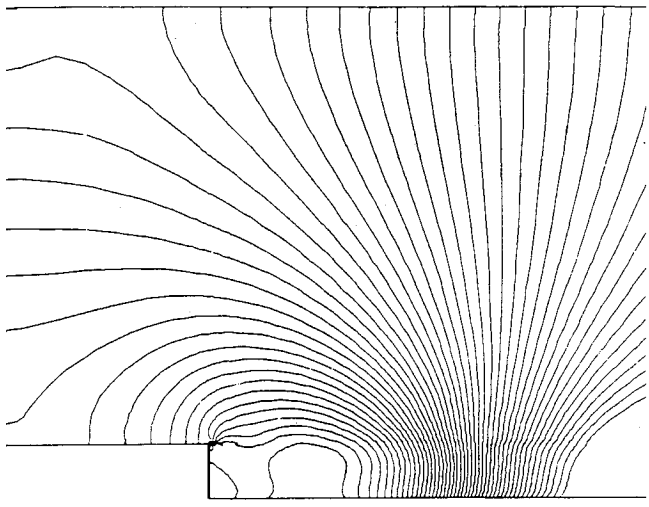

Fig. 5 Pressure contour.

and the eddy viscosity is given as

$$\nu_t = c_{\mu f}(k^2/\epsilon_p) \tag{9}$$

The turbulent kinetic energy equations, Eqs. (5) and (7), are defined for the entire flow domain while the energy transfer rate equation, the dissipation rate equation, and the eddy viscosity equation are valid for the flow domain away from the near-wall region. The turbulence model constants are given as $\sigma_{kp} = 0.75$, $\sigma_{kt} = 0.75$, $\sigma_{\epsilon p} = 1.15$, $\sigma_{\epsilon t} = 1.15$, $c_{p1} = 0.21$, $c_{p2} = 1.24$, $c_{p3} = 1.84$, $c_{t1} = 0.29$, $c_{t2} = 1.28$, and $c_{t3} = 1.66$.

The energy transfer rate and the dissipation rate inside the near-wall layer are given as

$$\epsilon_p = \epsilon_t = (\epsilon_1/f_\epsilon) \tag{10}$$

where $\epsilon_1 = c_{\mu f}^{3/4} k^{3/2}/\kappa y$, $f_\epsilon = 1 - \exp(-A_\epsilon R_t)$, $R_t = k^2/\nu\epsilon_1$, and $A_\epsilon = c_{\mu f}^{3/2}/2\kappa^2$. The dissipation rate given as Eq. (10) is formally identical to the one proposed by Wolfshtein.[17] For $y \approx 0$, Eq. (10) takes the limit value given as $2\nu k/y^2$, which is an analytical solution of the turbulent kinetic energy equation for a limiting case as y approaches the wall. Slightly away from the wall where the turbulence is in the equilibrium state, f_ϵ becomes unity. For near-wall equilibrium turbulent flows, the production rate (P_r) is approximately equal to the dissipation rate (ϵ_t) and hence the energy transfer rate (ϵ_p) from the low wave number production range to the high wave number dissipation range has to be approximately equal to the production and dissipation rates. Recall that the production rate vanishes on the wall and grows to a peak value at $y^+ \approx 15$. Hence Eq. (10) may not be a good approximation for $0 < y^+ < 15$. However, use of the vanishing boundary condition for the turbulent kinetic energy on the wall yields a growth rate of turbulent kinetic energy and a production rate that are in good agreement with measured data as well as theoretical analysis.[16] The eddy viscosity in the near-wall layer is given as

$$\nu_t = c_{\mu f} f_\mu (k^2/\epsilon_1) \tag{11}$$

where $f_\mu = 1 - 1/\exp(A_1\sqrt{R_t} + A_2 R_t^2)$ is a linear function of the distance from the wall in the viscous sublayer and becomes unity in the fully turbulent region. The $A_1 = 0.025$ and $A_2 = 0.00001$ are used for the near-wall layer.[16] The eddy viscosity given as Eq. (11) grows in proportion to the cubic power of the distance from the wall. It can be found in Ref. 16 that the near-wall analysis yields the same growth rate of the eddy viscosity in the region very close to the wall. For wall-bounded turbulent flows, the equilibrium region extends from $y^+ \approx 30$ to ≈ 300. Thus the partition between the near-wall region and the fully turbulent outer region can be located between $y^+ > 30$ and < 300 approximately. The present near-wall turbulence model is valid for the entire flow domain of equilibrium boundary-layer flows.[16] Thus the computational results do not depend strongly on the location of the partition. However, if the partition is located too far away from the wall, then the numerical results may become similar to those obtained using a k-equation turbulence model.

A few differences between the present M-S turbulence model and that of Hanjalic et al.[3] and Schiestel[4] are summarized here (see Ref. 15 for more details). First, the eddy viscosity equation in Hanjalic et al.[3] and Schiestel[4] is given as

$$\mu_t = \rho c_{\mu f}(k k_p/\epsilon_p) \tag{12}$$

Equation (12) implies that the small-scale eddies contained in the dissipation range may not contribute significantly to the turbulent transport of mass and momentum. This implication may not hold very well unless k_t is always negligibly small. However, in this case, the multiple-time-scale turbulence model can become a single-time-scale turbulence model.[3] Second, in the present M-S turbulence model, the variable energy transfer functions were obtained from a physical dimensional analysis.[24] On the other hand, the other M-S turbulence model[3,4] contains such a variable energy transfer function only in the energy transfer rate equation. Third, in the present M-S turbulence model, the model constants ($c_{p\ell}$, $c_{t\ell}$, $\ell = 1, 3$) were obtained by solving a five by five system of equations and by numerically optimizing one model constant ($c_{p\ell}$) to yield the

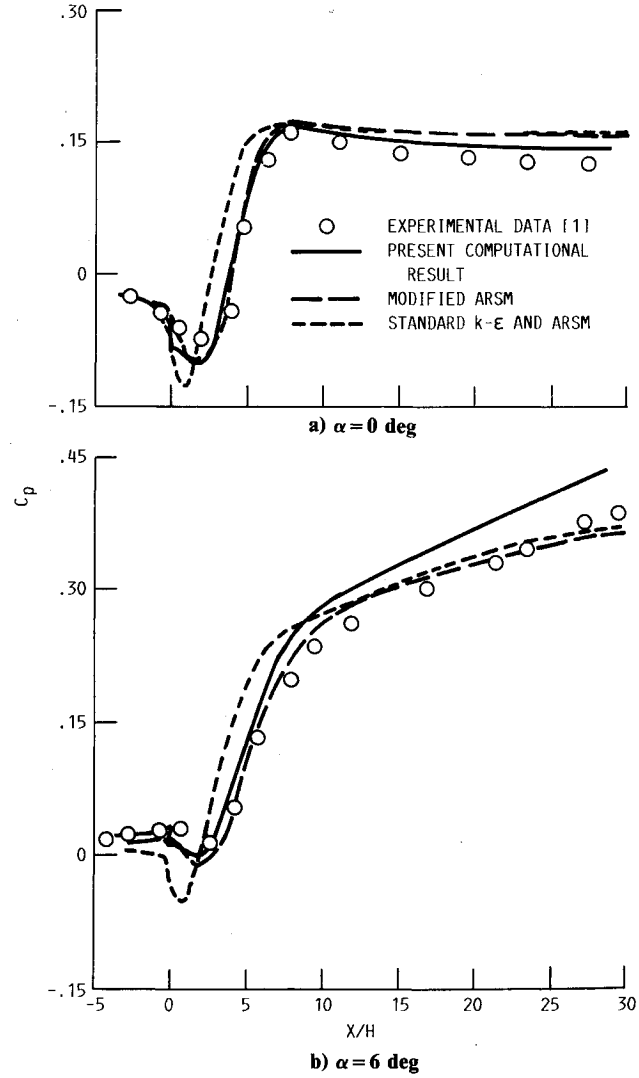

Fig. 6 Pressure on bottom wall.

best solutions for a fully developed channel flow and a plane jet exhausting into a moving stream.[2] One equation for the model constants is obtained from the equilibrium condition. Two equations are obtained by transforming the multiple-time-scale turbulence equations into asymptotic turbulence growth rate equations that are equivalent to that of Harris et al.[25] The other two equations are obtained by transforming the present turbulence equations into asymptotic turbulence decay rate equations that are equivalent to that of Harlow and Nakayama.[26] Last, of practical importance, arbitrary ratios of k_p/k_t were used as a near-wall boundary condition in application to complex turbulent flows.[3] This boundary condition is inconsistent with the near-wall analysis.[2] Also, an arbitrary ratio of k_t/k_p was used as an inlet boundary condition in a number of boundary-layer calculations.[3] In this case, the calculated shear layer expands rapidly so that the turbulence field can adjust itself to the ill-posed inlet boundary condition.[2]

Computational Results

The experimental data for the reattaching shear layer can be found in Ref. 1. The inlet freestream velocity is 40 m/s, the boundary-layer thickness is 0.019 m, and the height of the backward-facing step is 0.0127 m. The top wall was deflected from -2 to 10 deg to generate a strong adverse pressure gradient.

In numerical calculations, the inlet boundary was located at four step heights upstream of the expansion corner and the exit boundary was located at approximately 35 step heights downstream of the expansion corner. The flow domain was discretized by a 105×85 mesh with concentration of grid points near the expansion corner and in the bottom wall region. The sheared grid for the entire flow domain and that in the vicinity of the expansion corner for $\alpha = 6$ deg are shown in Fig. 2. It can be seen in the figure that the grid in the vicinity of the expansion corner is fine enough to resolve details of the large eddies subjected to strong shear and sudden expansion. The mesh for $\alpha = 0$ deg can be found in Ref. 27. The inlet boundary conditions for the tangential velocity, the turbulent kinetic energies, and the dissipation rates (ϵ_p and ϵ_t) were obtained from experimental data for a fully developed boundary-layer flow over a flat plate.[2,28] The nondimensional velocity and the turbulent kinetic energy profiles were scaled to yield a boundary-layer thickness of 0.019 m at the inlet boundary. The no-slip boundary condition for velocities and vanishing turbulent kinetic energies were prescribed at the solid wall boundary. At the exit boundary, a vanishing gradient boundary condition was used for all flow variables except the pressure. A uniform pressure was prescribed at the exit boundary. The use of vanishing gradient boundary conditions at the exit boundary may not be a good approximation for $\alpha \neq 0$. Thus the location of the exit boundary was moved downward until the numerical results in the region where the measured data and the calculated results are compared became almost independent of the location of the exit boundary. The numerical results in the upstream region, except for a few grid points near the exit boundary, were not significantly influenced by the exit boundary condition for the small top-wall

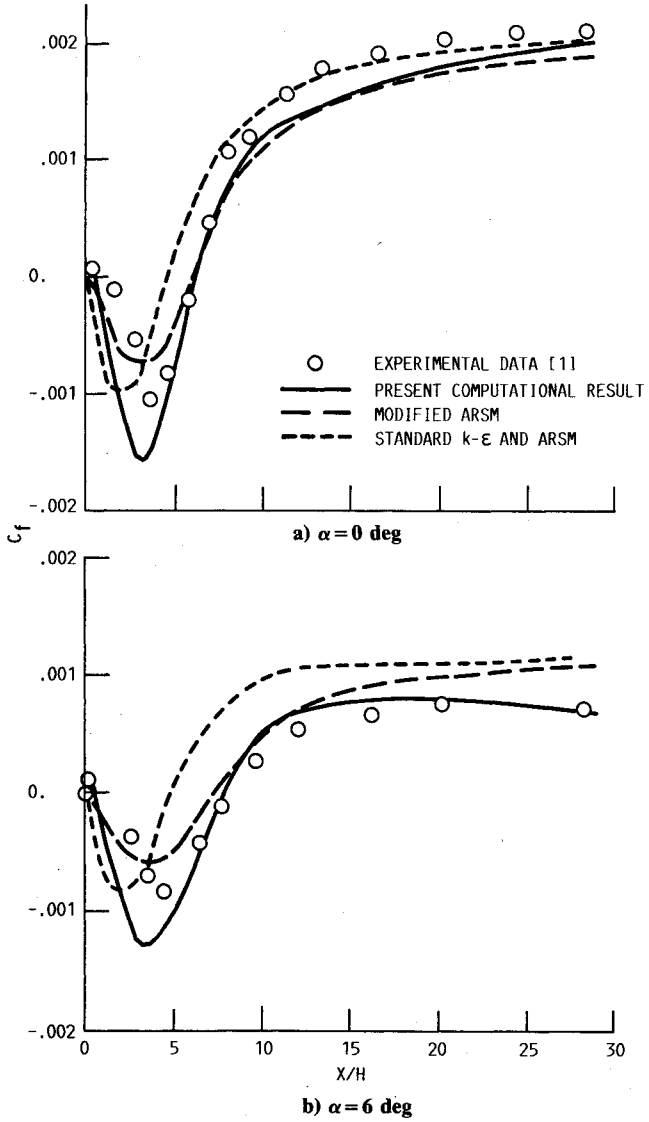

Fig. 7 Shear stress on bottom wall.

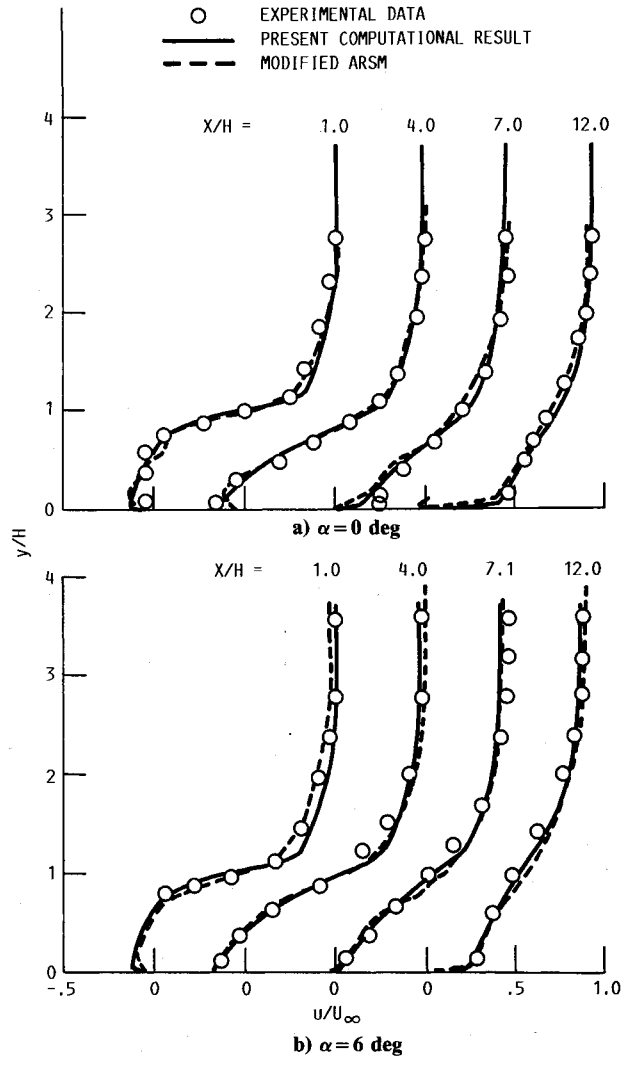

Fig. 8 Velocity profiles.

deflection angles. The partition between the near-wall layer and the external region was located at $y^+ \approx 100$, and 12 grid points were allocated inside the near-wall layer. The mesh size of the first grid point on the bottom wall was $\Delta y^+ \approx 2$, and the grid size in the normal to the wall direction was increased by a factor of approximately 1.15.

The calculated streamline contour is shown in Fig. 3. The flowfield consists of two recirculation zones. The primary recirculation zone extends from the separation corner toward the downstream direction, and the secondary recirculation zone is very small and is confined in the corner region. The reattachment location vs the top-wall deflection angle is shown in Fig. 4. It can be seen in the figure that the k-ϵ and ARSM turbulence models largely underpredict the reattachment location. The modified ARSM yields a significantly improved computational result; however, the results obtained using the M-S turbulence model are in better agreement with the measured data than those obtained using the modified ARSM. It is also shown in the figure that the k-ϵ model supplemented with the present near-wall turbulence model yields substantially improved results than do the standard k-ϵ and ARSM models, even though the results do not compare quite as favorably with the measured data as do those obtained using the M-S turbulence model and the modified ARSM.

The static pressure contour is shown in Fig. 5, where the pressure has been normalized by the inlet dynamic pressure and the incremental pressure between the contour lines is 0.005. It can be seen in the figure that a few contour lines pass

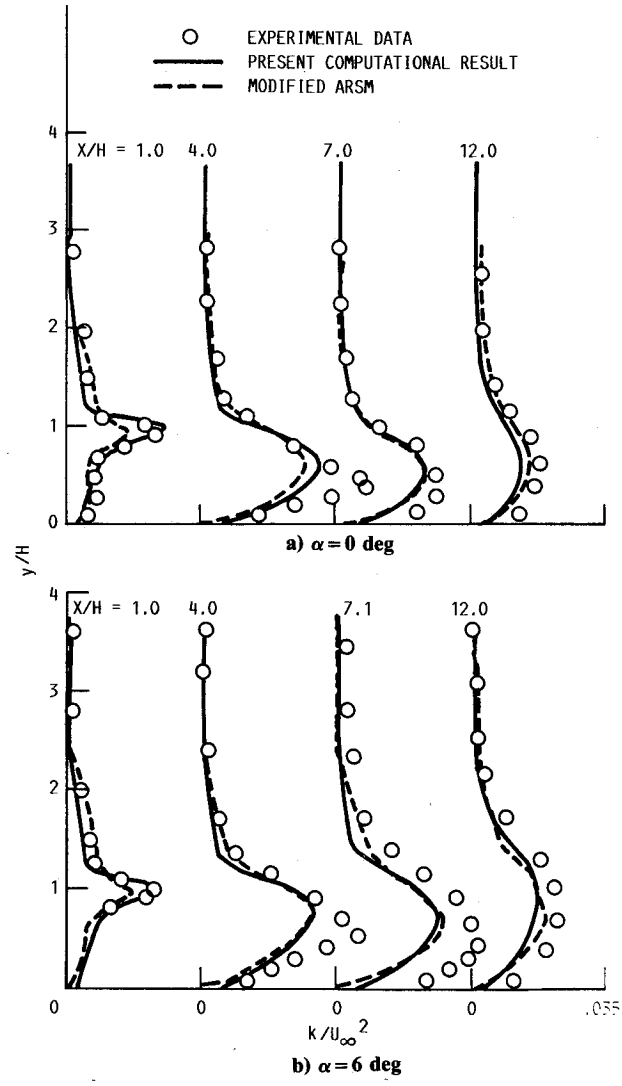

Fig. 9 Turbulent kinetic energy profiles.

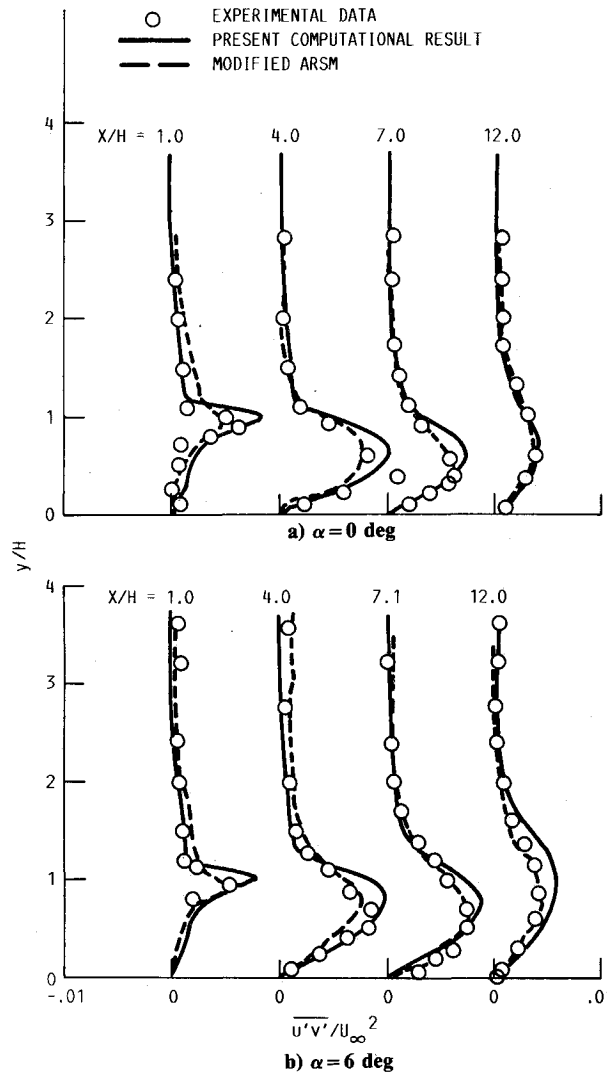

Fig. 10 Reynolds stress profiles.

through the expansion corner, and thus there exists a mild base pressure in the backward-facing step region. The calculated static pressure on the wall is compared with measured data as well as the numerical results of Ref. 1 in Fig. 6. The mild pressure drop at $x/H = 0$ represents the base pressure. For $\alpha = 0$ deg, the present computational result compares slightly more favorably with the measured wall pressure than does the other computational result. For $\alpha = 6$ deg, the M-S turbulence model overpredicts the wall pressure; however, the slope of the wall pressure in the continuously diverging downstream region obtained in the present study compares slightly more favorably with the measured data than the other results. This difference may be due to the use of different numerical methods.

The calculated wall-shearing stresses are shown in Fig. 7. It can be seen in the figure that the location of the peak wall-shearing stress obtained using the k-ϵ turbulence model is grossly in error. It is interesting to note that the modified ARSM underpredicts the peak values, and the present turbulence model overpredicts the peak values, even though the relative differences are almost the same for both deflection angles.

The mean velocity, the turbulent kinetic energy, and the Reynolds stress profiles at four downstream locations are compared with measured data and with the calculated results using the modified ARSM[1] in Figs. 8-10, respectively. The measured turbulent kinetic energy shown in Fig. 9 was estimated using the measured value of $\overline{u'^2 + v'^2}$ and an assumption that $\overline{w'^2} = (\overline{u'^2 + v'^2})/2$. As shown in Figs. 8-10, both

computational results exhibit good comparison with the measured data. It can be seen in Fig. 9 that the peak value of the turbulent kinetic energy and the shape of the turbulent kinetic energy profile obtained using the M-S turbulence model compare slightly better with the measured data than do those obtained using the modified ARSM at $x/H = 1.0$ where the turbulence is in a strong nonequilibrium state. At locations further downstream, the present computational results compare slightly less favorably with the measured data than do the results obtained using the modified ARSM. However, the differences between the two numerical results are negligible, as can be seen in these figures.

The ratio of turbulent kinetic energy in production range to that in dissipation range at a few downstream locations are shown in Fig. 11. It can be seen in the figure that the ratio of k_p/k_t for $\alpha = 0$ deg near the expansion corner is slightly greater than that for $\alpha = 6$ deg, which indicates that the level of nonequilibrium for $\alpha = 0$ deg is slightly greater than that for $\alpha = 6$ deg. This result is attributed to the slightly higher production rate caused by the slightly higher mean velocity gradient for $\alpha = 0$ deg than that for $\alpha = 6$ deg near the expansion corner. It can be seen in the figure that the ratio of k_p/k_t for $\alpha = 6$ deg is higher than that for $\alpha = 0$ deg in most of the flow domain and that the peak value of k_p/k_t for $\alpha = 6$ deg is slightly skewed upward than that for $\alpha = 0$ deg. These results indicate that the nonequilibrium region extends further across the flow domain as the top-wall deflection angle is further increased. Here, the k_p/k_t in the near-wall region does not necessarily represent the strength of nonequilibrium since the closure level of the near-wall turbulence model is the same as the k-equation turbulence model.

The ratio of turbulent viscosity to molecular viscosity at three downstream locations is shown in Fig. 12. It can be seen in the figure that the Jones-Launder k-ϵ turbulence model and the M-S turbulence model predict a relatively small turbulent viscosity in the region very close to the bottom wall and that these calculated results are in good agreement with the measured data. At locations slightly away from the bottom wall ($y/H \approx 0.5$), the Jones-Launder k-ϵ turbulence model overpredicts the turbulent viscosity so that the reattachment location is largely underpredicted. On the other hand, the present computational results compare quite favorably with the measured data so that the reattachment location is correctly predicted. This indicates that the improved numerical results are more attributed to the M-S turbulence model than to the near-wall turbulence model. The calculated production and dissipation rates of the turbulent kinetic energy at the same downstream locations were qualitatively and quantitatively almost the same as those of Ref. 1.

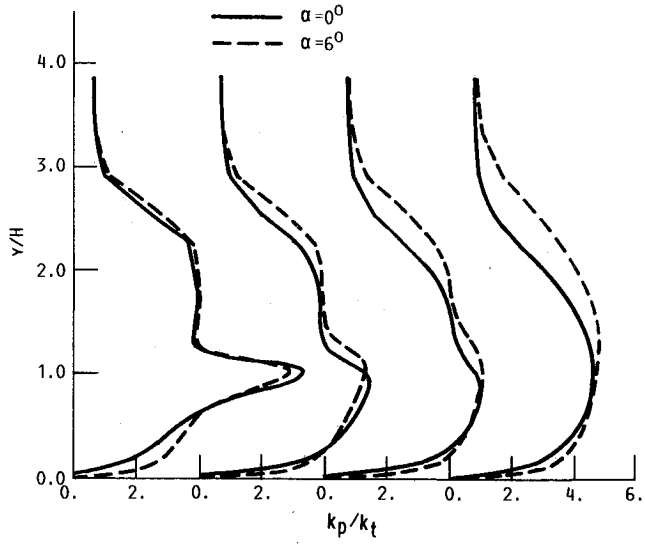

Fig. 11 The kp/k_t profiles.

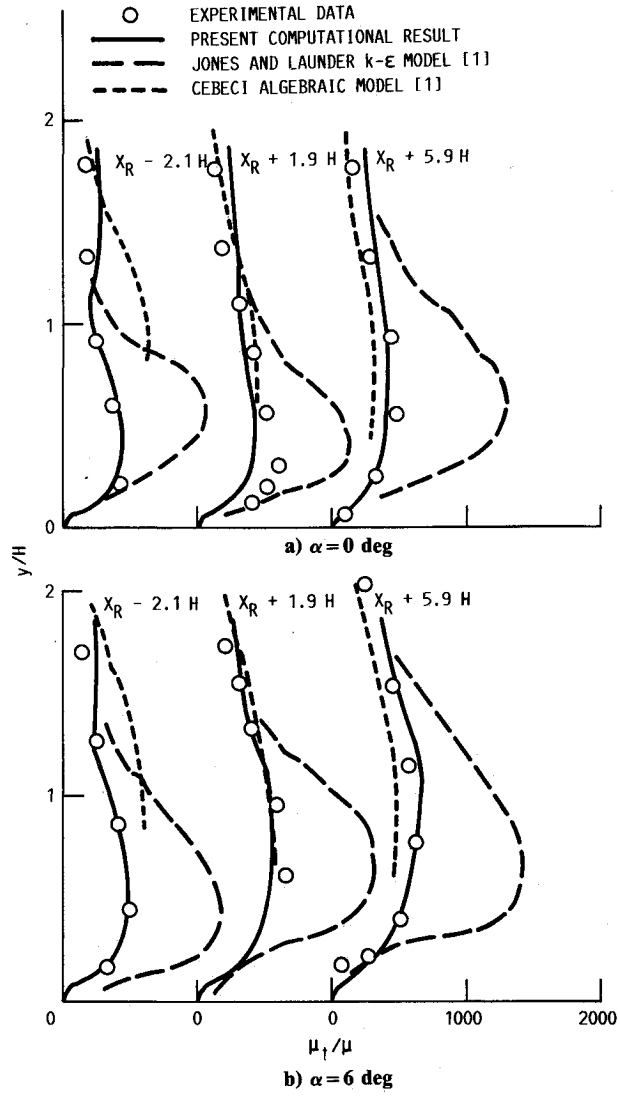

Fig. 12 The μ_t/μ profiles.

Conclusions

Numerical calculations of reattaching shear layers in a diverging channel using a multiple-time-scale turbulence model supplemented with a near-wall turbulence model have been presented. The calculated reattachment location vs the top-wall deflection angle is in good agreement with the measured data. The prediction of the correct reattachment location is attributed to the calculated turbulent viscosity that is in good agreement with the measured data, and the correct prediction of the turbulent viscosity is attributed to the capability of the multiple-time-scale turbulence model to resolve the nonequilibrium turbulence field in the vicinity of the expansion corner and in the following shear-layer region. The calculated wall pressure and the wall-shearing stress are also in good agreement with the measured data. The rest of the computational results such as the normalized velocity profiles and the Reynolds stress profiles compare favorably with the measured data. The computational results obtained using the multiple-time-scale turbulence model compare slightly more favorably with the measured data than do those obtained using the modified algebraic Reynolds stress turbulence model.

The capability of the multiple-time-scale turbulence model to resolve the strong nonequilibrium turbulence field is attributed to the use of the multiple time scales. Recall that the turbulent transport of mass and momentum is governed by the time scale of energy containing large eddies, and the dissipation of turbulent kinetic energy is governed by the time scale of fine-scale eddies in the dissipation range.[29] In the multiple-

time-scale turbulence model, the turbulent transport of mass and momentum is described using the time scale of the large eddies, and the dissipation rate is described using the time scale of the fine-scale eddies. The improved computational result obtained using the multiple-time-scale turbulence model for complex turbulent flows is attributed to the physically consistent nature of the turbulence model.

References

[1]Driver, D. M., and Seegmiller, H. L., "Features of a Reattaching Turbulent Shear Layer in Divergent Channel Flow," *AIAA Journal*, Vol. 23, No. 2, 1985, pp. 163–171.

[2]Kim, S.-W., and Chen, C.-P., "A Multiple-Time-Scale Turbulence Model Based on Variable Partitioning of the Turbulent Kinetic Energy Spectrum," *Numerical Heat Transfer*, Pt. B, Vol. 16, No. 2, 1989, pp. 193–211; also, NASA CR-179222, Nov. 1988.

[3]Hanjalic, K., Launder, B. E., and Schiestel, R., "Multiple-Time-Scale Concepts in Turbulent Shear Flows," *Turbulent Shear Flows*, Vol. 2, edited by L. J. S. Bradbury, F. Durst, B. E. Launder, F. W. Schmidt, and J. H. Whitelaw, Springer-Verlag, New York, 1980, pp. 36–49.

[4]Schiestel, R., "Multiple-Time-Scale Modeling of Turbulent Flows in One Point Closure," *Physics of Fluids*, Vol. 30, No. 3, 1987, pp. 722–731.

[5]Wilcox, D. C., "Multiscale Model for Turbulent Flows," *AIAA Journal*, Vol. 26, No. 11, 1988, pp. 1311–1320.

[6]Wilcox, D. C., "Reassessment of the Scale-Determining Equation for Advanced Turbulence Models," *AIAA Journal*, Vol. 26, No. 11, 1988, pp. 1299–1310.

[7]Irwin, H. P. A. H., "Measurements in a Self-Preserving Plane Wall Jet in a Positive Pressure Gradient," *Journal of Fluid Mechanics*, Vol. 61, Pt. 1, 1973, pp. 33–63.

[8]Tsiolakis, E. P., Krause, E., and Muller, U. R., "Turbulent Boundary Layer-Wake Interaction," *Turbulent Shear Flows*, Vol. 4, edited by L. J. S. Bradbury, F. Durst, B. E. Launder, F. W. Schmidt, and J. H. Whitelaw , Springer-Verlag, New York, 1983, pp. 204–215.

[9]Kim, J., Kline, S. J., and Johnston, J. P., "Investigation of a Reattaching Turbulent Shear Layer: Flow over a Backward-Facing Step," *Journal of Fluids Engineering*, Vol. 102, Sept. 1980, pp. 302–308.

[10]Roback, R., and Johnson, B. V., "Mass and Momentum Turbulent Transport Experiments with Confined Swirling Coaxial Jets," NASA CR-168252, Aug. 1983.

[11]Bradshaw, P., "Effects of Streamline Curvature on Turbulent Flow," AGARDograph 169, 1973.

[12]Baskaran, V., Smits, A. J., and Joubert, P. N., "A Turbulent Flow over a Curved Hill; Part I Growth of an Internal Boundary Layer," *Journal of Fluid Mechanics*, Vol. 182, Sept. 1987, pp. 47–83.

[13]Kim, S.-W., "Numerical Investigation of an Internal Layer in Turbulent Flow over a Curved Hill," NASA TM-102230, Oct. 1989.

[14]Johnson, D. A., "Transonic Separated Flow Prediction with an Eddy-Viscosity/Reynolds-Stress Closure Model," *AIAA Journal*, Vol. 25, No. 2, 1987, pp. 252–259.

[15]Kim, S.-W., "Numerical Investigation of Separated Transonic Turbulent Flows with a Multiple-Time-Scale Turbulence Model," NASA TM-102499, Jan. 1990.

[16]Kim, S.-W., "A Near-Wall Turbulence Model and Its Application to Fully Developed Turbulent Channel and Pipe Flows," *Numerical Heat Transfer*, Pt. B, Vol. 17, Jan. 1990, pp. 101–122; also, NASA TM-101399, Nov. 1988.

[17]Wolfshtein, M., "The Velocity and Temperature Distribution in One-Dimensional Flow with Turbulence Augmentation and Pressure Gradient," *International Journal of Heat and Mass Transfer*, Vol. 12, 1969, pp. 301–318.

[18]Chen, H. C., and Patel, V. C., "Practical Near-Wall Turbulence Models for Complex Flows Including Separation," AIAA Paper 87-1300, June 1987.

[19]Roshko, A., "Structure of Turbulent Shear Flows: A New Look," *AIAA Journal*, Vol. 14, No. 10, 1976, pp. 1349–1357.

[20]Kim, S.-W., "A Control-Volume Based Reynolds Averaged Navier-Stokes Equation Solver Valid at All Flow Velocities," NASA TM-101488, Feb. 1989.

[21]Kim, S.-W., "Numerical Computation of Shock Wave-Turbulent Boundary Layer Interaction in Transonic Flow over an Axisymmetric Curved Hill," NASA TM-101473, Feb. 1989.

[22]Patankar, S. V., *Numerical Heat Transfer and Fluid Flow*, McGraw-Hill, New York, 1980.

[23]Vanka, S. P., Chen, B. C. J., and Sha, W. T., "A Semi-Implicit Calculation Procedure for Flows Described in Boundary Fitted Coordinate System," *Numerical Heat Transfer*, Vol. 3, No. 1, 1980, pp. 1–19.

[24]White, F. M., *Viscous Fluid Flow*, McGraw-Hill, New York, 1974.

[25]Harris, V. G., Graham, J. A. H., and Corrsin, S., "Further Experiments in Early Homogeneous Turbulent Shear Flow," *Journal of Fluid Mechanics*, Vol. 81, 1977, pp. 657–687.

[26]Harlow F. H., and Nakayama, P. I., "Transport of Turbulence Energy Decay Rate," Los Alamos Scientific Lab., Los Alamos, NM, LA-3854, Feb. 1968.

[27]Kim, S.-W., "Calculation of Reattaching Shear Layers in Divergent Channel with a Multiple-Time-Scale Turbulence Model," AIAA Paper 90-0047, Jan. 1990

[28]Klebanoff, P. S., "Characteristics of Turbulence in a Boundary Layer with Zero Pressure Gradient," NACA Rept. 1247, 1955.

[29]Lumley, J. L., "Turbulence Modelling," *Journal of Applied Mechanics*, Vol. 50, Dec. 1983, pp. 1097–1103.